



Suppressing channel-shortening effect of self-aligned coplanar Al-doped In-Sn-Zn-O TFTs using Mo-Al alloy source/drain electrode as Cu diffusion barrier

Wooseok Jeong^a, Jörg Winkler^b, Hennrik Schmidt^c, Kwang-Heum Lee^a, Sang-Hee Ko Park^{a,*}

^a Department of Materials Science and Engineering, Korea Advanced Institute of Science and Technology (KAIST), 291 Daehak-ro, Yuseong-gu, Daejeon 305-701, Republic of Korea

^b PLANSEE SE, 6600 Reutte, Austria

^c PLANSEE (Shanghai) High Performance Material Ltd, Shanghai, China

ARTICLE INFO

Article history:

Received 17 September 2020

Received in revised form 24 November 2020

Accepted 5 December 2020

Available online 10 December 2020

Keywords:

MoAl alloy

Cu diffusion barrier

Self-aligned coplanar TFT

High-mobility

Hydrogen diffusion

ABSTRACT

Developing high-resolution displays to achieve realistic images have been in a great demand recently regardless of the display size. However, in the backplane technology, the channel-shortening effect is a serious obstacle in realizing oxide thin film transistors (TFTs) with short channel lengths. In this study, we investigated the channel-shortening effect of Al-doped InSnZnO (Al:ITZO) thin-film transistors (TFTs) with Mo and Mo-based alloy Cu diffusion barriers and proposed Mo–Al alloy as a Cu diffusion barrier to effectively reduce the channel-shortening effect. The TFTs with the Mo (Cu diffusion barrier) exhibited negative V_{on} shifts and a channel-shortening length (ΔL) of 3.52 μm at an annealing temperature of 290 °C, although no chemical reaction occurred at the Mo/Al:ITZO interfaces. In addition, the TFTs with the Mo–Ti (Cu diffusion barrier) showed the largest ΔV_{on} and ΔL values at various annealing temperatures. The material and electrical analysis results confirmed that the hydrogen diffusion from the source/drain region is the main cause of the channel-shortening effect. Thus, the TFTs with the Mo–Al (Cu diffusion barrier) exhibited excellent characteristics against the channel-shortening effect by forming a uniform and thin Al_2O_3 layer at the Mo–Al/Al:ITZO interface and preventing the hydrogen diffusion. The ΔV_{on} remained almost unchanged, and the ΔL was 1.61 μm up to an annealing temperature of 290 °C. This study suggests a highly beneficial method for producing oxide TFTs, while suppressing the channel-shortening effect by tailoring the interface between source/drain and active layer using an appropriate Cu diffusion electrode.

© 2020 Elsevier B.V. All rights reserved.

1. Introduction

Recently, amorphous oxide semiconductor (AOS) thin-film transistors (TFTs) have attracted considerable attention owing to their advantages such as high transparency, low off-current, good uniformity, and scalability [1–3]. Therefore, AOS TFTs are promising candidates for the backplane technologies of flat panel displays (FPDs). Many studies have been conducted recently on active layers, gate dielectrics, and metal electrodes. For example, for high capacitance and low operating voltage, hafnium-based high-k gate dielectric materials have been studied for the application to the MOSFET [4–7]. Above all, with the development of displays towards large size and high resolution, it has become important to have fast response times

for switching TFTs to reduce the charge/discharge time of capacitors. Hence, there have been many studies on oxide TFTs with high mobility materials such as indium zinc oxide (IZO) [8], indium oxide (In_2O_3) [9], indium tin zinc oxide (ITZO) [10], and N or Al-doped indium tin zinc oxide (Al:ITZO) [11–14]. Cho et al. reported backchannel etch (BCE) oxide semiconductor TFTs using Al-doped tin-zinc-indium oxide (Al:ITZO), that showed high mobility and high etch selectivity in PAN-based wet chemical etchant [11]. Among the various types of oxide TFT structures, self-aligned top gate (SA-TG) coplanar TFTs offer the advantages of low parasitic capacitance based on negligible gate to source/drain overlap and better channel length scalability. This enables a much faster display operating frame rate compared to the bottom gate staggered structures, which is desirable for high-resolution active-matrix organic light-emitting diode (AMOLED) display applications [15–17]. Since, copper (Cu) has lower resistivity than aluminum (Al), it is generally preferred for electrodes to minimize the resistor-capacitor (RC) delay [18,19]. Although both Cu and Al

* Corresponding author.

E-mail address: shkp@kaist.ac.kr (S.-H.K. Park).

electrodes with metal-oxide layer show good ohmic contact property, Cu exhibits advantages over Al in terms of resistance to the electromigration (transport of atoms caused by high current densities) and mechanical stress endurance because of higher atomic mass. In addition, Cu shows good solderability and low cost compared to Al [20–24]. However, Cu easily diffuses into the adjacent active layer, degrading the device characteristics [24,25]. Thus, molybdenum and molybdenum alloys are often used as Cu diffusion barriers by inserting layers between the Cu electrode and active layer to suppress the Cu diffusion [26,27]. Another important issue related to high-resolution displays is maximizing the aperture ratio for the pixel downsizing. Therefore, realizing TFTs with short channel lengths is crucial for high-resolution displays. However, there are some issues to be resolved in downsizing oxide TFTs owing to the channel-shortening effect ($\Delta L = L_{ch} - L_{eff}$) due to the carrier diffusion from other layers [17]. The origin of carrier diffusion is known to be the combined effects of V_o generation at the interface of the S/D and active layer and H diffusion from the passivation layer or inter-layer dielectric (ILD) [28–31]. Although there have been many studies on the channel-shortening effect of oxide TFTs, only few studies have reported the effects of S/D electrodes on the effective channel length. In particular, the origin of the channel-shortening effect of molybdenum (the most commonly used electrode) is still controversial because no chemical reaction occurs at the interface between molybdenum and the IGZO active layer [32–34]. Since there is no oxide layer at the Mo/IGZO interface, no oxygen vacancies (V_o) get formed; thus, the investigation on the source of channel-shortening remains unclear. Furthermore, most of the research on the channel-shortening effect is related to IGZO-based TFTs than high-mobility oxide TFTs [17,29,35]. Because a

high-mobility oxide semiconductor such as Al-doped ITZO has a higher carrier concentration than IGZO, the effective channel length ($L_{eff} = L_{ch} - \Delta L$) can be easily reduced even with a slight diffusion of carriers. Therefore, the control of the channel-shortening length is particularly important in high-mobility oxide TFTs.

In this study, we investigated in detail the ΔL ($L_{ch} - L_{eff}$) of high mobility Al-doped amorphous ITZO top gate coplanar self-aligned TFTs using different Cu diffusion barriers (Mo, Mo–Ti, Mo–Al) with a stacked Cu/Cu barrier S/D electrodes. First, the ΔL of the Mo and Mo–Ti (Cu diffusion barriers) was exhibited by the transmission line method (TLM) at different annealing temperatures. Through various analysis methods, we demonstrated the effect of the S/D electrodes (Cu/Cu diffusion barriers) on the channel-shortening effect, and the most influential factor was identified. Considering the investigated origin of the channel-shortening effect, as an appropriate Cu diffusion barrier material, Mo–Al, was employed to suppress the cause of ΔL . With Mo–Al, as a Cu diffusion barrier, ΔL reduced significantly and hardly altered under the annealing conditions. This method has significant advantages of controlling the channel-shortening effect by simply changing the Cu diffusion barrier electrodes. This suggests a simple manufacturing method for TFTs that works reliably with a short channel.

2. Experimental method

2.1. Fabrication process of top gate coplanar self-aligned Al:ITZO TFTs

Fig. 1a shows a schematic image of top gate coplanar self-aligned TFTs. First, Al-doped ITZO was deposited by RF sputtering, followed by patterning as an active layer. SiO_2 and molybdenum were

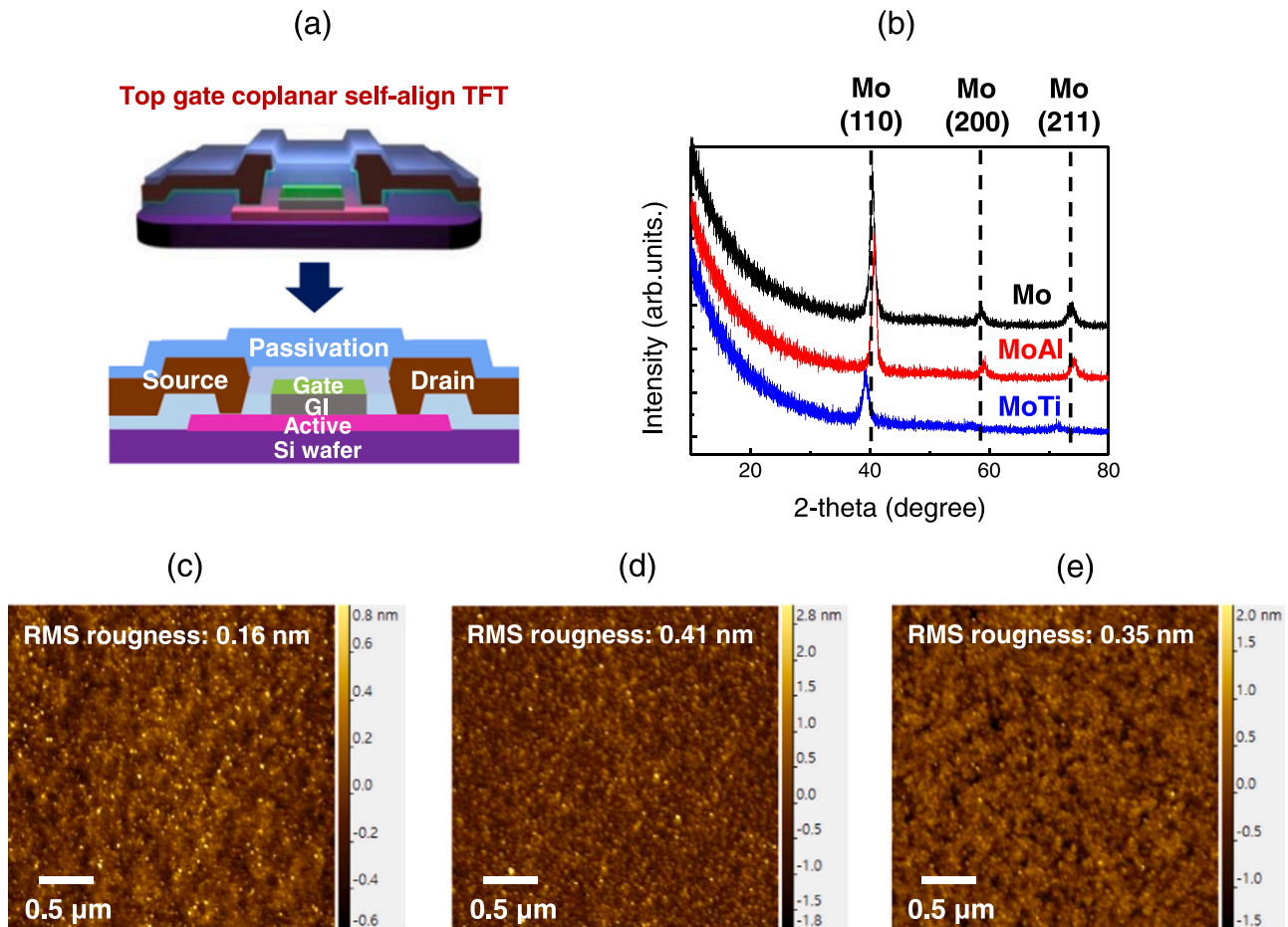


Fig. 1. (a) Schematic image of top gate self-aligned structured TFT and (b) XRD results of Cu diffusion barriers (Mo, Mo–Ti, Mo–Al). AFM topography image of (c) Mo, (d) Mo–Ti and (e) Mo–Al films.

deposited by plasma-enhanced chemical vapor deposition (PECVD) and sputtering for the gate insulator (GI) and gate electrode, respectively. After patterning the gate electrode, the exposed SiO₂ gate insulator was dry-etched using the gate electrode as a mask. The exposed Al:ITZO section of the source/drain region was treated with Ar plasma for 60 s at 100 W to form n⁺-doped source/drain extension regions. A 200 nm thick SiO₂ film as an inter-layer dielectric (ILD) was then deposited by PECVD, followed by dry etching for the source/drain contact hole. Next, copper and copper diffusion barriers were deposited and patterned as the source/drain electrodes. In this work, molybdenum (Mo, Device A), molybdenum-titanium (Mo-Ti, Device B), and molybdenum-aluminum (Mo-Al, Device C) were used as the copper diffusion barriers. Finally, Al₂O₃ was deposited by thermal ALD (T-ALD) as the passivation layer. To deposit the Al₂O₃ layer, trimethylaluminum (TMA) precursor and H₂O were used as the aluminum and oxygen sources, respectively. After the fabrication of self-aligned TFTs, the samples were annealed from 230 °C to 290 °C to observe the changes in V_{on} and channel-shortening length with different S/D Mo alloy Cu diffusion barriers.

2.2. Characterization of self-aligned TFTs with different Mo alloys as Cu diffusion barriers

To measure the electrical properties of Al:ITZO self-aligned TFTs, a precision LCR meter (Agilent 4284A) and semiconductor parameter analyzer with a probe station (HP 4156A) were used. X-ray diffraction (XRD) measurements were performed with an X'Pert-PRO MRD diffractometer at a film thickness of 30 nm. To measure the topography image and RMS roughness, AFM measurements were carried out at ambient conditions (23–24 °C and 46–50% relative humidity) using a Park XE-100 (Park Systems) instrument. Besides, a field emission transmission electron microscope (JEM-2100F HR) was used to examine the cross-sectional images between Cu diffusion barriers (Mo, Mo-Ti, Mo-Al) and Al:ITZO layers at different annealing temperatures. X-ray photoelectron spectroscopy (XPS) measurements were performed under ultra-high vacuum (10⁻⁹ Torr) equipped with an Al K α X-ray source (Thermo VG Scientific). The chemical bonding states of the Mo, Mo-Ti, and Mo-Al/Al:ITZO interfaces were investigated by XPS depth profiling with Ar ion sputtering. To determine the hydrogen diffusion from Al₂O₃ layer to Al:ITZO film, a secondary ion mass spectrometry, MS-SIMS (IMS 7f, CAMECA) was used with a Cs⁺ primary ion beam with a current of 15 nA and raster size of 250 μ m \times 250 μ m.

3. Results and discussion

Fig. 1b shows the XRD patterns of the three different Cu diffusion barriers under the investigation. All barrier films were polycrystalline and exhibited only body-centered cubic (bcc)-related peaks of molybdenum. This indicated that all thin films consist of molybdenum-based solid solutions. It was observed that compared to the diffraction peaks of the Mo films, the Mo-Ti films peaks shifted to lower diffraction angles, indicating an increase in the lattice parameter of the Mo-Ti films. In contrast, the diffraction peaks of the Mo-Al films shifted to higher diffraction angles, showing a reduction in the lattice parameter owing to the replacement of molybdenum by aluminum with a smaller atom size. Fig. 1(c)–(e) show AFM topography image of Cu barrier materials of Mo, Mo-Ti and Mo-Al films with the thickness of 30 nm, respectively. RMS (root-mean square) roughness of Mo, Mo-Ti and Mo-Al films is 0.16, 0.41 nm, and 0.35 nm, respectively. SIMS results in Fig. S1 show the Cu diffusion property in the Al:ITZO film before and after the annealing process at 290 °C. Regardless of the annealing process, a negligible intensity of Cu was observed in the Al:ITZO film with the Mo, Mo-Ti, and Mo-Al films, indicating excellent Cu diffusion barrier properties.

To investigate the electrical properties of the top gate coplanar self-aligned Al:ITZO TFTs, the transfer characteristics are measured, as shown in Fig. 2. The applied V_{DS} was 0.1 V and the channel width (W) and length (L) were set to 8 μ m and 4 μ m, respectively. Devices with Cu diffusion barriers of Mo (device A), Mo-Ti (device B) and Mo-Al (device C) exhibited high field-effect mobilities (more than 30 cm² V⁻¹ s⁻¹), low subthreshold swing (Vdec⁻¹), and low hysteresis (V) in the as-fabricated condition. The representative transfer parameters of each device are listed in Table 1.

The field effect mobility (μ_{FE}) was calculated at a V_{DS} of 0.1 V in the linear region by the following equation

$$\mu_{FE} = \frac{g_m}{\frac{W}{L} \times C_i \times V_d} \left(\text{where } g_m \equiv \frac{\partial I_d}{\partial V_g} \right)$$

where W and L are the channel width and length, respectively, and g_m is the transconductance at a low drain voltage. The turn-on voltage (V_{on}) was determined by the V_{gs} where I_d = W/L \times 10 pA at a V_{DS} of 0.1 V and subthreshold swing (SS) value was extracted by the following equation

$$SS = \frac{\partial V_G}{\partial(\log I_{DS})}$$

Fig. 2a and b show the transfer characteristics of the devices A (Mo) and B (Mo-Ti) after annealing at different temperatures. The device B shows more V_{on} shifts in the negative direction with increasing annealing temperature than device A (Mo) does, as shown in Fig. 2b. The large V_{on} shift along the subsequent annealing process indicated an increased carrier concentration in the channel region. Considering that all TFTs were fabricated in the same process except for the materials of Cu diffusion barrier electrodes in the source/drain regions, the differences in V_{on} shifts originated from the Cu diffusion barrier electrodes deposited in the source/drain extension regions. Therefore, device B getting conductive after annealing at 250 °C indicated that the carrier concentration in the channel increased drastically, resulting in the TFT to lose gate control ability. The output characteristics were measured at small V_D (V_D = -1 V ~ 1 V) to observe the ohmic contact resistance of device A (Mo) and B (Mo-Ti). It showed the typical behavior of the output curve with no current crowding, indicating good ohmic contact properties (Fig. 2c and d).

To quantitatively investigate the channel-shortening length (ΔL) due to lateral carrier diffusion from source/drain extension regions, the transmission line method (TLM) was employed. It is a widely used method for extracting the channel-shortening length, contact resistance, and channel resistance [36–38]. The I-V characteristics of TFT is expressed as following equation:

$$I_D = \frac{W}{L - \Delta L} \mu C_{OX} \left\{ (V_G - V_T) - \frac{1}{2} V_D \right\} V_D$$

I_D, W, L_{eff} (= L- ΔL), μ , C_{OX}, V_G, V_T, and V_D indicated the drain current, channel width, effective channel length, mobility, gate oxide capacitance, gate voltage, threshold voltage, and drain voltage, respectively. The channel resistance (R_{ch}) can be expressed as

$$R_{ch} = \frac{V_D}{I_D} = \frac{L - \Delta L}{W \mu C_{OX} (V_G - V_T - \frac{1}{2} V_D)}$$

Because the total resistance (R_{tot}) is the sum of the channel resistance and the contact resistance,

R_{tot} = R_{ch} + R_C, R_{tot} is expressed by the following equation:

$$R_T = \frac{V_{DS}}{I_D} = R_{ch} + R_C = \frac{L - \Delta L}{\mu_{FE} \cdot C_{OX} \cdot W \cdot (V_{GS} - V_T - \frac{V_{DS}}{2})} + R_C$$

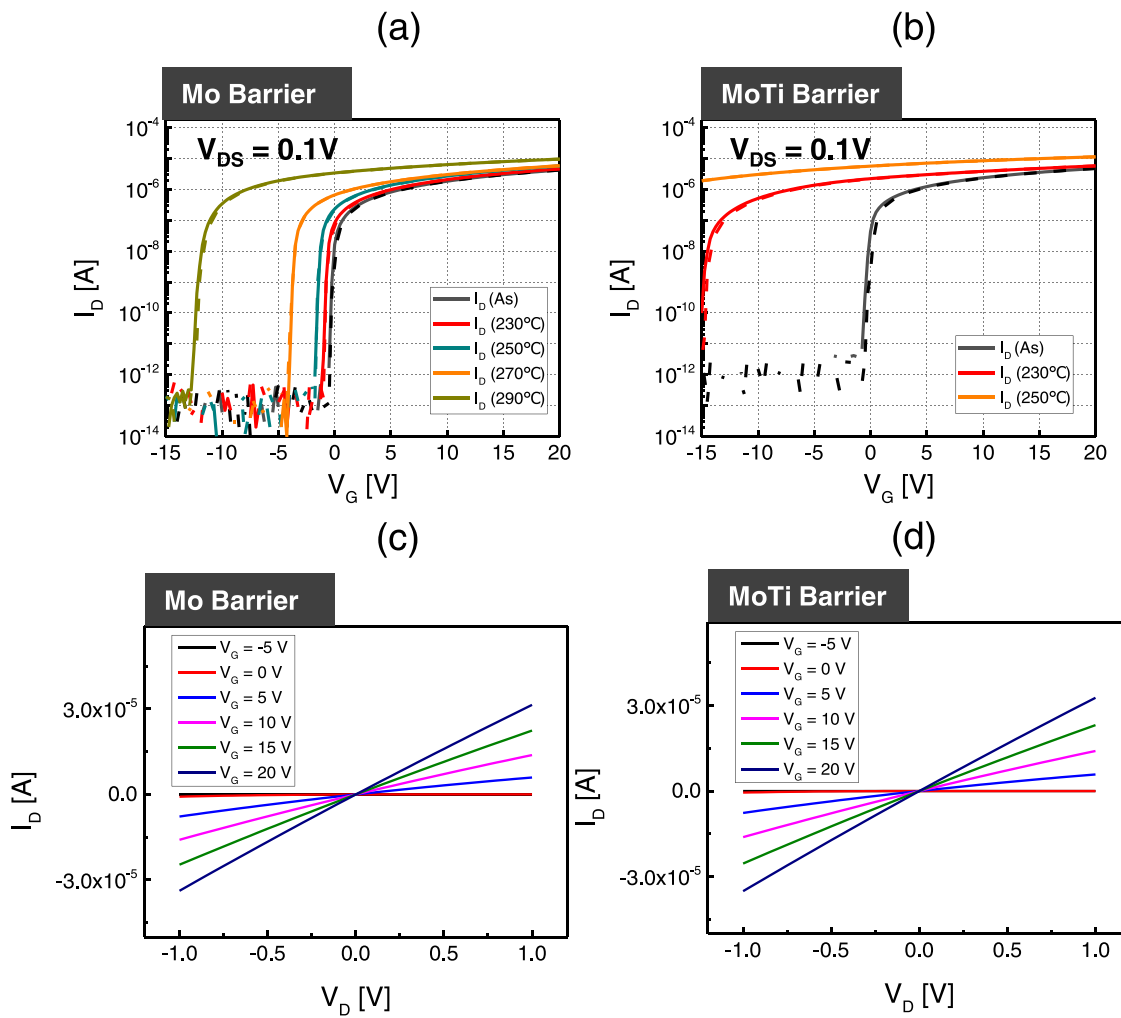


Fig. 2. Transfer characteristics of (a) device A (Mo barrier) and (b) device B (Mo-Ti barrier). Output characteristics of (c) device A (Mo barrier) and (d) device B (Mo-Ti barrier).

In the TLM results, $V_{GS}-V_{ON}$ was used instead of $V_{GS}-V_T$. The fitted line for each $V_{GS}-V_{ON}$ converges at one point, where the X and Y coordinates are ΔL and contact resistance (R_C), respectively.

Fig. 3 shows width-normalized total resistance ($W \cdot R_T$) with respect to channel length set at 4, 6, 10, and 20 μm , measured at $V_{DS} = 0.1\text{ V}$ for various $V_{GS}-V_{ON}$ ($= 3, 4, 6, 8, 10, \text{ and } 12\text{ V}$). Fig. 3a, b, and c show the width-normalized total resistance ($R_T \times W$) as a function of L and $V_{GS}-V_{ON}$ for device A (Mo) at different annealing temperatures. The measured ΔL for the as-fabricated device and device annealed at 250 $^\circ\text{C}$ and 290 $^\circ\text{C}$ were 0.94, 1.4, and 3.52 μm , respectively. On the contrary, device B (Mo-Ti) exhibited ΔL of 1.54 μm for as-fabricated device, and already 3.8 μm for the device annealed at 230 $^\circ\text{C}$, indicating a short effective channel length than the device A (Mo) (Fig. 3a, b, and c). Because the device B (Mo-Ti) exhibited conductive characteristics above the annealing temperature of 250 $^\circ\text{C}$, the TLM was only calculated up to a temperature of 230 $^\circ\text{C}$. Considering that the channel-shortening length (ΔL) is due to the lateral carrier diffusion from the S/D extension region, the degrees of change in V_{on}

(Fig. 2a and b) and channel-shortening length (Fig. 3a, b, c, d, and e) with annealing temperature showed a similar behavior.

To investigate the differences in ΔV_{on} and ΔL for devices A and B, high-resolution TEM (HRTEM) images were obtained for the interface between the Cu diffusion barriers (Mo, Mo-Ti) and Al:ITZO layers. Fig. 4 shows the TEM images of the Mo/Al:ITZO interface of the as-deposited and annealed samples at 290 $^\circ\text{C}$. The cross-sectional HRTEM images in Fig. 4a and b clearly demonstrate that no chemical reaction occur between the Mo and Al:ITZO interface for as-deposited and annealed sample at 290 $^\circ\text{C}$. Because the formation energy of Mo oxide (MoO_2 ($\Delta H_{\text{MoO}_2} = -533.2\text{ kJ/mol}$)) is higher than that of In_2O_3 ($\Delta H_{\text{In}_2\text{O}_3} = -925.8\text{ kJ/mol}$), Mo does not form a compound with Al:ITZO film at the Mo/Al:ITZO interface even after the annealing process. XPS depth profiling was performed to investigate in detail the interfacial reaction at the Mo/Al:ITZO interface. The Mo 3d core-level spectra of the Mo and Al:ITZO interfacial regions for the as-deposited and annealed samples are shown in Fig. 4c. The binding energies of Mo 3d_{3/2} and 3d_{5/2} doublets were 227.7 eV and 231.0 eV, respectively, indicating the only peak of a molybdenum metal. This revealed that Mo oxide does not exist at the Mo/Al:ITZO interface [39]. The cross-sectional HRTEM images and XPS depth results show no clear evidence of molybdenum forming an oxide between the Mo and the Al:ITZO layer. However, as shown in Figs. 2a and 3a, b, and c, the V_{on} shifts to the negative direction and ΔL increases with increasing annealing temperature for device A even without the Mo oxide formation. This means that the oxygen vacancy (V_o) is not the origin of the channel-shortening effect in device

Table 1

Electrical characteristics parameters of each device (Device A, B, C).

	μ_{FE} ($\text{cm}^2\text{V}^{-1}\text{s}^{-1}$)	V_{on} (V)	S.S (Vdec ⁻¹)
Device A (Mo)	33.99	-0.5	0.09
Device B (Mo-Ti)	32.31	-0.75	0.11
Device C (Mo-Al)	34.46	-0.5	0.11

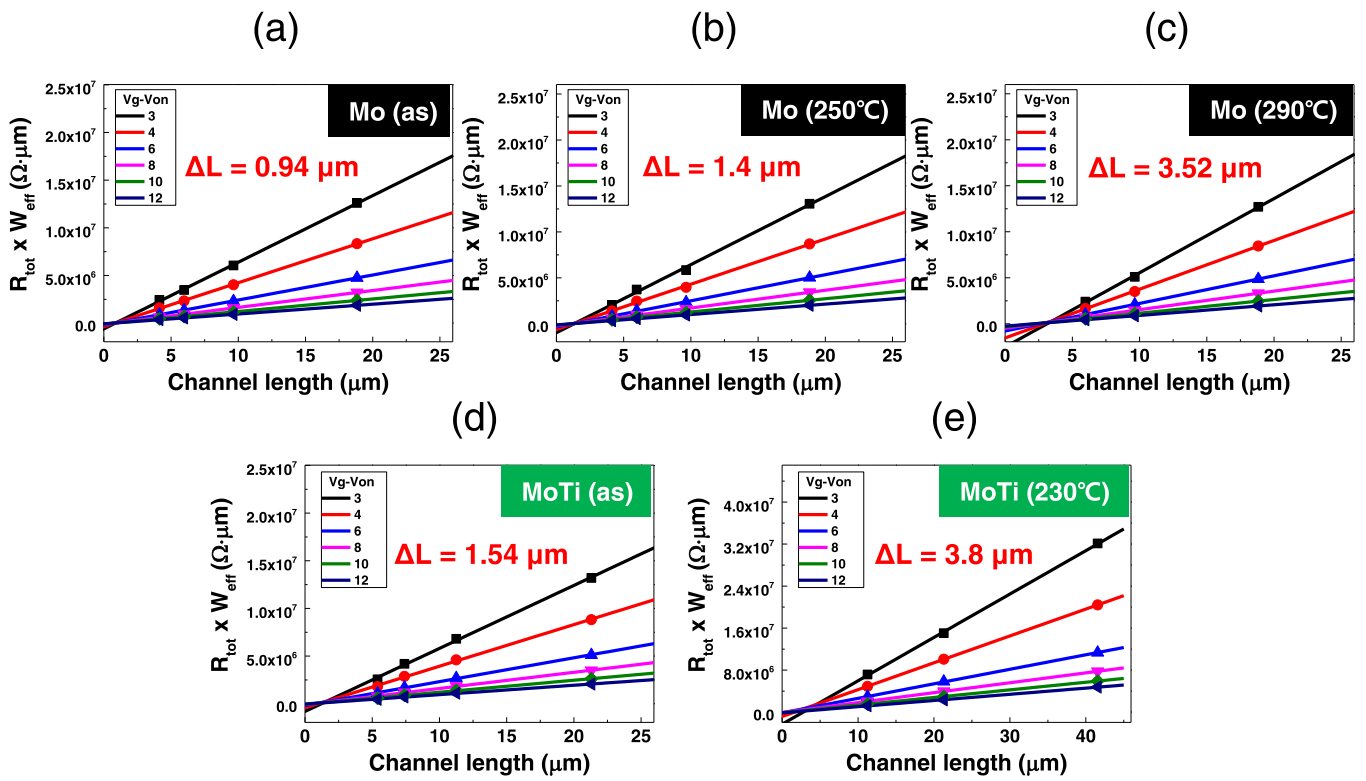


Fig. 3. TLM analysis of device A (Mo barrier) for the (a) as-deposited and (b) annealed at 250 °C and (c) 290 °C. TLM analysis of device B (Mo-Ti barrier) for the (d) as-deposited and (e) annealed at 230 °C.

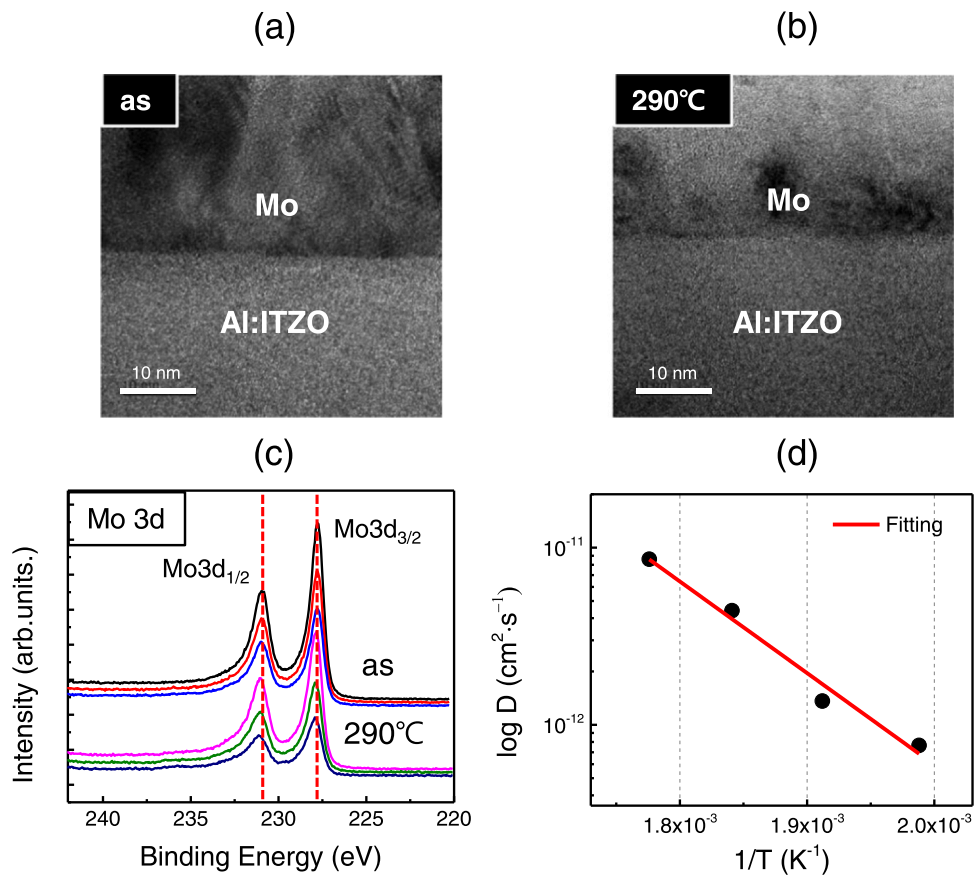


Fig. 4. Cross-sectional TEM images of the (a) as-deposited Mo/Al:ITZO interfaces and (b) Mo/Al:ITZO interfaces annealed at 290 °C. (c) Mo 3d level spectra of the XPS depth profiles measured at Mo/Al:ITZO interfaces for as-deposited and annealed at 290 °C. (d) Arrhenius plot of diffusion coefficient obtained from the ΔL results of device A (Mo barrier).

A, rather other carrier sources are injected into the active layer. To scrutinize this further, we extracted activation energy from the diffusion coefficient. Using the extracted ΔL from the TLM measurement as shown in Fig. 3a, b, and c, the diffusion coefficient is calculated from the diffusion length expressed as $(\Delta L)^2 = D \cdot t$. Because ΔL indicated the channel length reduction from both sides, $\Delta L/2$ was used as the diffusion length. The diffusion coefficients for 230, 250, 270, and 290 °C were 7.6×10^{-13} , -1.3×10^{-12} , -4.4×10^{-12} , -8.6×10^{-12} cm²/s, respectively. The diffusion coefficient was plotted as a function of annealing temperature by using the Arrhenius equation, $D = D_0 \exp(-\frac{E_a}{kT})$. From the slope of graph in Fig. 4d, the activation energy (E_a) can be obtained. The extracted activation energy was 0.44 eV, which was comparable to the activation energy of the hydrogen diffusion coefficient (0.3 – 1.2 eV) surrounded with Zn atoms [40,41]. This suggested that the hydrogen diffusion from S/D region is the main reason for the channel-shortening effect of device A.

In addition to Mo, the TEM images and enlarged TEM lattice images were also acquired to measure the reaction between the Mo-Ti (Cu diffusion barrier) and Al:ITZO. Fig. 5a shows a TEM image and enlarged lattice image of the as-deposited Mo-Ti/Al:ITZO interface. In the TEM image, a crystalline phase was observed at the Al:ITZO region indicating that certain chemical reactions occurred at the Mo-Ti/Al:ITZO interface. The enlarged TEM lattice image indicated the inter-planar spacing value (d -value) of 0.28 nm (2.8 Å), which is close to the d -value of indium and tin metal for the (111) and (200) plane, respectively. (JCPDS card No. 05–0642, 04–0673). The formation energy of TiO₂ is ($\Delta H_{\text{TiO}_2} = -944.0$ kJ/mol) lower than that of In₂O₃

($\Delta H_{\text{In}_2\text{O}_3} = -925.8$ kJ/mol). Therefore, TiO_x can be formed at the interfacial region between Mo-Ti and Al:ITZO layers by taking oxygen from Al:ITZO, resulting in indium and tin metal lattice fringe. The TEM and enlarged lattice images in Fig. 5b represent the Mo-Ti/Al:ITZO interface annealed at 290 °C. The annealed Mo-Ti/Al:ITZO interface also exhibited crystallinity at the Al:ITZO region, and a d -value of 0.28 nm (2.8 Å) was observed in the enlarged lattice image, same as that in Fig. 5a. However, compared to the as-fabricated Mo-Ti/Al:ITZO sample (Fig. 5a), a region with the crystalline phase was more widely observed in the Al:ITZO film annealed at 290 °C. This indicated the titanium diffusion into the Al:ITZO layer by taking the oxygen bound to the indium and tin atoms during the annealing process. Thus, the Al:ITZO layer was reduced by titanium oxidation. Fig. 5c shows Ti2p level spectra of XPS depth profiles obtained from the as-fabricated and annealed Mo-Ti/Al:ITZO interfaces. The binding energies of Ti2p_{3/2} and Ti2p_{1/2} were observed at 458.8 eV and 464.1 eV, respectively, corresponding to the Ti2p core level spectra of titanium oxide (TiO₂) [42]. These results correspond to the TEM results, wherein titanium oxide (TiO₂) is formed at the interface between the Mo-Ti and Al:ITZO layers through a chemical reaction [34,39].

According to other studies, the formation of titanium oxide at the Mo-Ti/Al:ITZO interface contributes to the increased carrier concentration in the Al:ITZO layer due to the oxygen vacancies (V_o) [28,39,43]. Therefore, we obtained the XPS O1s spectra of the Mo/Al:ITZO and Mo-Ti/Al:ITZO interfaces annealed at 250 °C (Fig. 6a and b). The O1s spectra were deconvoluted into three sub-peaks as Gaussian distributions. The three different sub-peaks correspond to

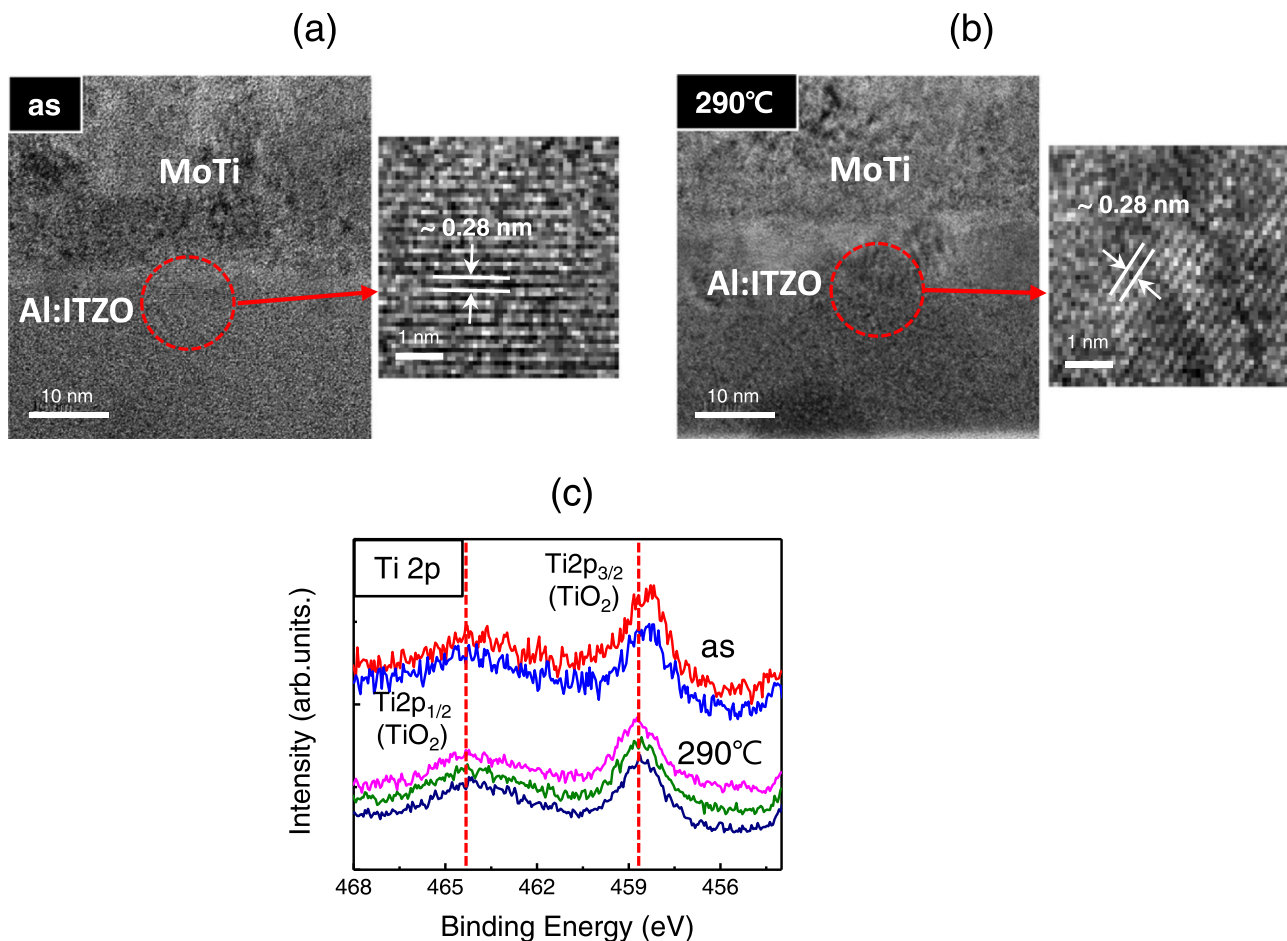


Fig. 5. (left) Cross-sectional TEM images, (right) enlarged TEM images for the selected areas in the TEM images of Mo-Ti/Al:ITZO interfaces for the (a) as-deposited and (b) annealed at 290 °C. (c) Ti 2p level spectra of the XPS depth profiles measured at Mo-Ti/Al:ITZO interfaces for the as-deposited and annealed at 290 °C.

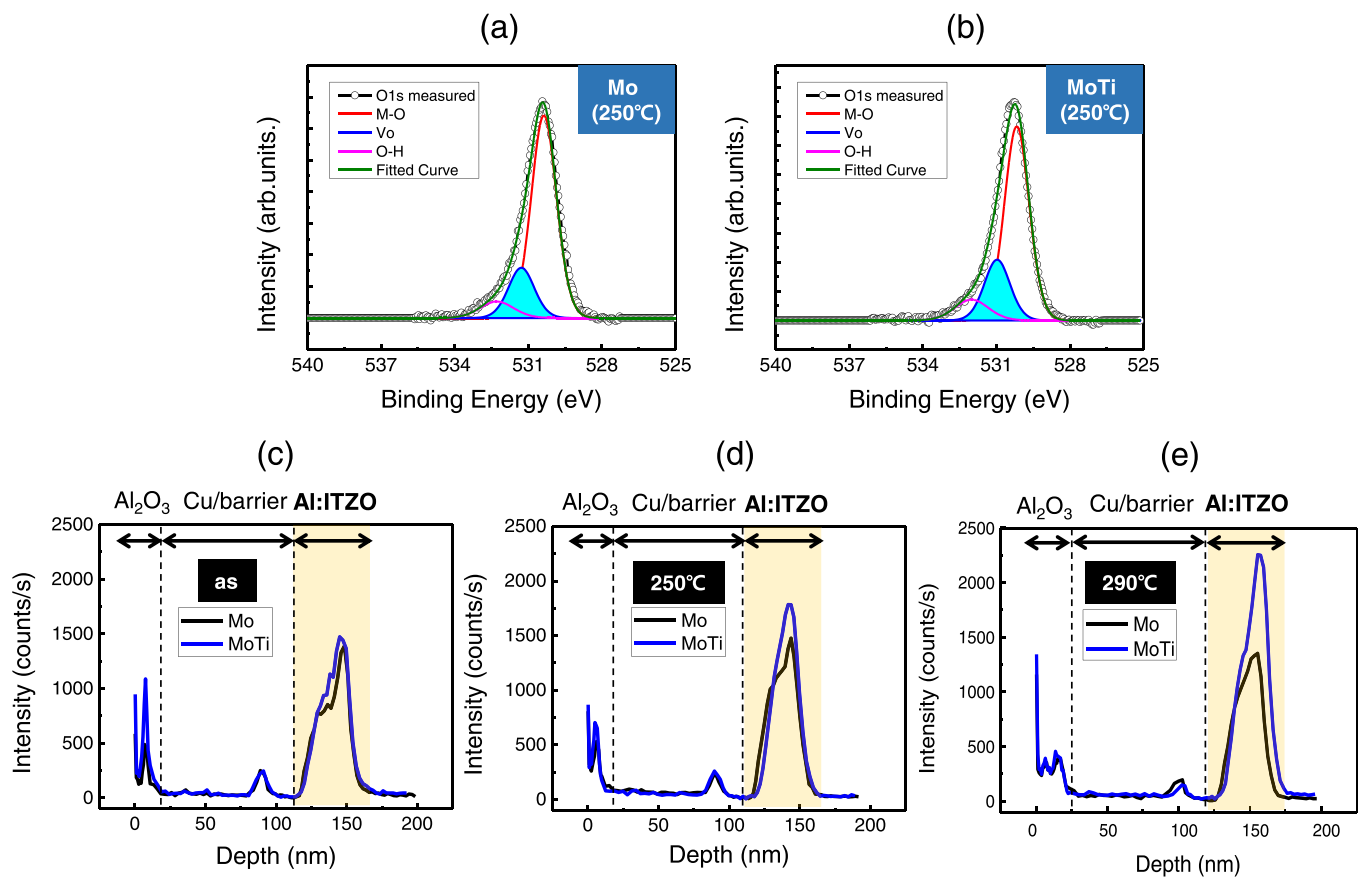
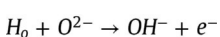


Fig. 6. XPS O1s peaks and de-convoluted peaks of (a) Mo/Al:ITZO interface and (b) Mo-Ti/Al:ITZO interface annealed at 250 °C. Depth profile of -OH element in (c) as-deposited stacked film and after thermal annealing process at a temperature of (d) 250 °C and (e) 290 °C.

metal-oxygen bonds (M-O, 530.15 ± 0.02 eV), oxygen-deficiency (V_o , 531.01 ± 0.04 eV), and oxygen-hydrogen bonds (O-H, 532.03 ± 0.02 eV) [44,45]. The Mo-Ti/Al:ITZO sample annealed at 250 °C exhibited only a 2.35% increase in the area related to the oxygen-deficient (V_o) region compared to the Mo/Al:ITZO sample annealed at 250 °C. Nevertheless, as shown in Fig. 2b, even at the annealing condition of 250 °C, the device B (Mo-Ti) become conductive, while the device A (Mo) exhibit -1.25 V of ΔV_{on} . Considering that the ΔV_{on} and ΔL differences between the devices A (Mo) and B (Mo-Ti) are too large, the contribution of oxygen vacancy (V_o) to the increased carrier concentration is relatively small. As previously explained from the results of device A (Mo), the channel-shortening effect can ascribe to the hydrogen diffusion from the S/D region.

To investigate the hydrogen diffusion from the S/D metal to the Al:ITZO layer, the depth profiles of the H and OH contents were investigated using SIMS measurements. The depth profile of the H (Fig. S2) content of a film with the same stack sequence as the S/D region of the transistor indicated almost the same amount of hydrogen in the Al:ITZO layer regardless of the type of Cu diffusion barrier. In contrast, the -OH compositions varied significantly with annealing temperatures between the samples with Mo and Mo-Ti (Fig. 6c, d, and e). As the annealing temperature increased, the -OH content in the Al:ITZO layer with the Mo-Ti (Cu diffusion barrier) rapidly increased compared to the sample with the Mo (Cu diffusion barrier). The hydrogen diffused into Al:ITZO layer from S/D region and bonded with O in the form of hydroxyl group (OH) during the annealing process. The incorporation of hydrogen results in electron doping by the following reaction [46,47]:



Thus, electrons created by -OH bonds increase the carrier concentration in the Al:ITZO layer. Since Ti is well known to have the ability to store more hydrogen than other metals, large amounts of hydrogen in Mo-Ti alloys are considered to affect the increase of -OH in the Al:ITZO layer [48]. To investigate the hydrogen content in the Cu diffusion barrier metals, elastic recoil detection (ERD) with 2.0 MeV was conducted as shown in Fig. S3. The calculated amount of hydrogen indicates Mo-Ti alloy has one order of magnitude higher than Mo and Al:ITZO. Therefore, hydrogen in Mo-Ti alloy diffuses into the Al:ITZO layer, which can be accelerated by heat treatment. However, the amount of hydrogen in Mo shows a similar value to that of Al:ITZO, so that the diffusion of hydrogen from Mo to Al:ITZO will hardly occur. Therefore, we consider the Al_2O_3 passivation layer as a hydrogen source because it contains large amounts of hydrogen originating from H_2O reactant during the thermal ALD (T-ALD) deposition process [49]. To investigate the effects of Al_2O_3 passivation layer on hydrogen diffusion into the active layer, the depth profile of the amount of -OH was investigated using SIMS measurement as shown in Fig. S4. The film was prepared with a same stack sequence as S/D region without Al_2O_3 passivation layer. At the annealing temperature of 250 °C, the amount of -OH in the Al:ITZO layer with Mo-Ti (Cu diffusion barrier) is increased. However, it is decreased again at the temperature of 290 °C while Al:ITZO layer having Mo (Cu diffusion barrier) exhibits a similar amount of -OH regardless of annealing temperatures. Fig. S5 indicates the transfer characteristics of the self-aligned TFTs without Al_2O_3 passivation layer. Almost no change of V_{on} was observed in the TFTs with Mo (Cu diffusion barrier). Considering the results of Fig. 2a that device A (Mo) which has Al_2O_3 passivation layer shows negative ΔV_{on} with annealing temperatures, we assume Al_2O_3 passivation layer serves as the source of

hydrogen. However, TFTs with Mo-Ti (Cu diffusion barrier) shows about negative -7 V of V_{on} shifts at the temperature of 250 °C, and positive 3.5 V of V_{on} shifts at 290 °C. This is because hydrogen contained in the Mo-Ti alloy diffuses into the active layer at 250 °C, and diffuse out again at 290 °C. This is the comparative results that device B (Mo-Ti) shows large negative V_{on} shifts even at the temperature of 230 °C as shown in Fig. 2b. From these results, we confirmed that the Al_2O_3 passivation layer serves as hydrogen source as well as acts as the barrier to prevent the out diffusion of hydrogen.

To suppress the channel-shortening effect caused by the hydrogen diffusion, we proposed applying the Mo-Al alloy as a Cu diffusion barrier. We anticipated that an ultra-thin Al_2O_3 layer would be formed at the Mo-Al/Al:ITZO interface through a chemical reaction, which acts as a hydrogen diffusion barrier from the S/D to the Al:ITZO layer because Al_2O_3 layer is an excellent passivation layer due to its ability to suppress gas permeation [50,51]. The transfer characteristics of device C (Mo-Al) is shown in Fig. S6. The applied V_{DS} is 0.1 and 10 V, respectively. The electrical characteristics such as field-effect mobility (μ_{FE}), subthreshold swing (S.S), and V_{on} were $34.46 \text{ cm}^2 \text{ V}^{-1} \text{ s}^{-1}$, 0.11 Vdec^{-1} , and -0.5 V , respectively as shown in Table 1. In addition, the on-off current ratio (I_{on}/I_{off}) was 1.47×10^7 . Fig. 7a shows the transfer characteristics of device C (Mo-Al) annealed at each temperatures. There was only a -0.25 V change in V_{on} until the annealing temperature reached 290 °C. The changes in V_{on} of the TFTs with different Cu diffusion barriers (Mo, Mo-Ti, Mo-Al) are shown in Fig. 7b as a function of annealing temperature. The changes in V_{on} were strongly dependent on the material of Cu

diffusion barrier electrode in the S/D region. The smallest ΔV_{on} was observed in device C (Mo-Al) as the annealing temperature increased. In addition, the transfer characteristics according to various channel widths (W) and lengths (L) were measured with each Cu diffusion barrier (Mo, Mo-Ti, Mo-Al). It exhibits the same trend of ΔV_{on} with the previous results as shown in Fig. S7. This suggested that some chemical reaction prevents the diffusion of hydrogen between the Mo-Al and Al:ITZO interface. The ΔL extracted by TLM was 0.29, 1.24, and 1.61 μm for the as-fabricated and annealed device at the temperatures of 250 °C and 290 °C, respectively, which were the smallest values compared to those of the device with other diffusion barriers.

To further investigate the reaction at the interface between the Mo-Al and Al:ITZO, TEM and XPS experiments were conducted. Fig. 8a and b show cross-sectional TEM images of the Mo-Al/Al:ITZO sample for the as-fabricated and annealed samples at 290 °C. The TEM images show a very thin Al_2O_3 formed at between the Mo-Al and Al:ITZO interfaces that became clearer at higher annealing temperature. This newly formed Al_2O_3 layer was also identified by the XPS depth profile measured at the Mo-Al/Al:ITZO interfaces (Fig. 8c). The binding energy of 74.6 eV in the Al 2p level spectra of the XPS depth profiles originating from the aluminum oxide (Al_2O_3) confirmed the formation of aluminum oxide film as well as TEM image between the Mo-Al and Al:ITZO interfaces. Moreover, the Al_2O_3 layer became thicker and denser at the 290 °C heat treatment, improving its ability to prevent hydrogen diffusion. Therefore, even under the annealing conditions where hydrogen diffusion is likely to occur, the Al_2O_3 layer formed at the Mo-Al/Al:ITZO interfaces

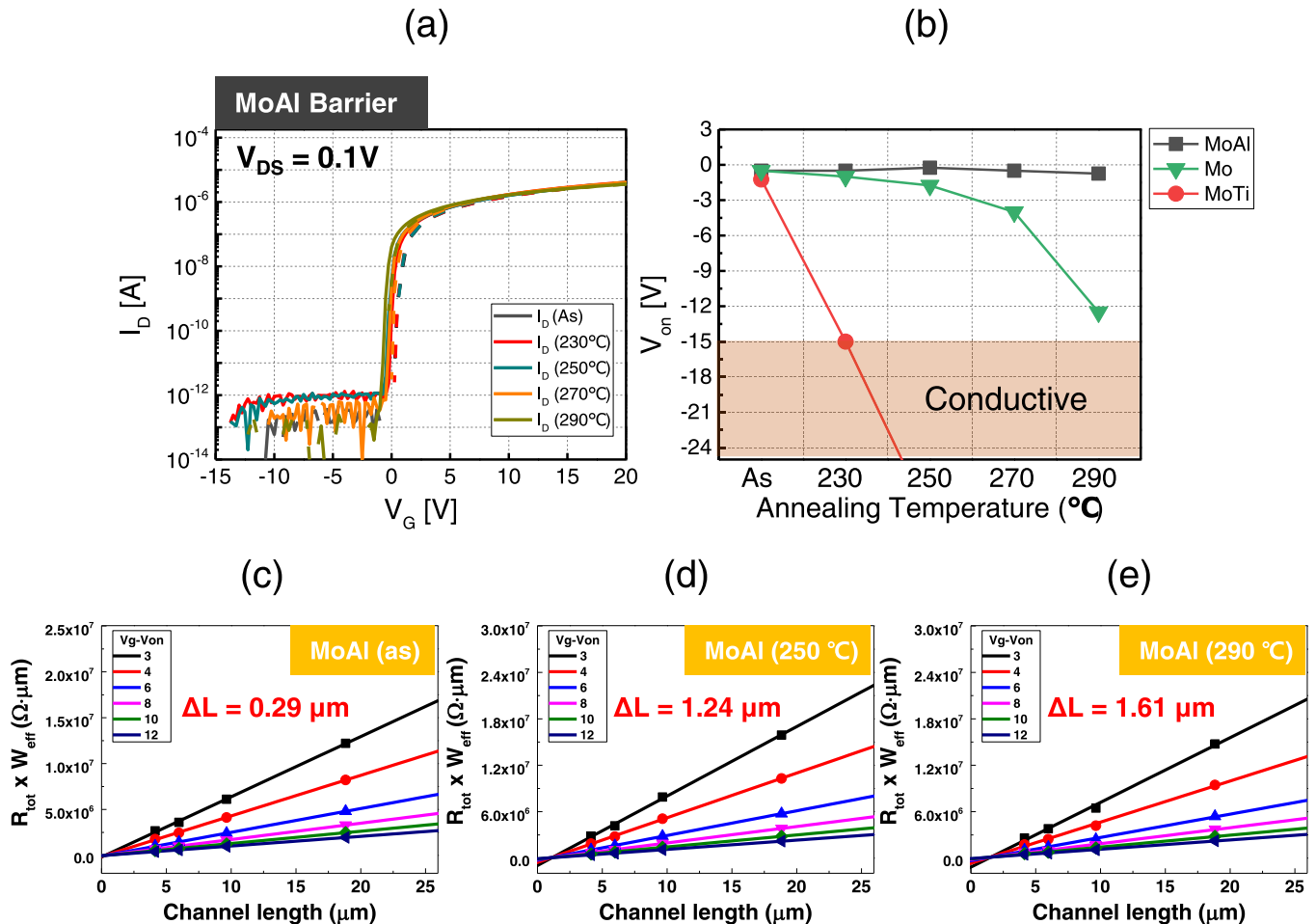


Fig. 7. (a) Transfer curve of device C (Mo-Al barrier) and (b) plot of the V_{on} shift of each devices (A, B, C) as a function of annealing temperature. TLM analysis of device C (Mo-Al barrier) for the (c) as-fabricated and annealed at (d) 250 °C and (e) 290 °C.

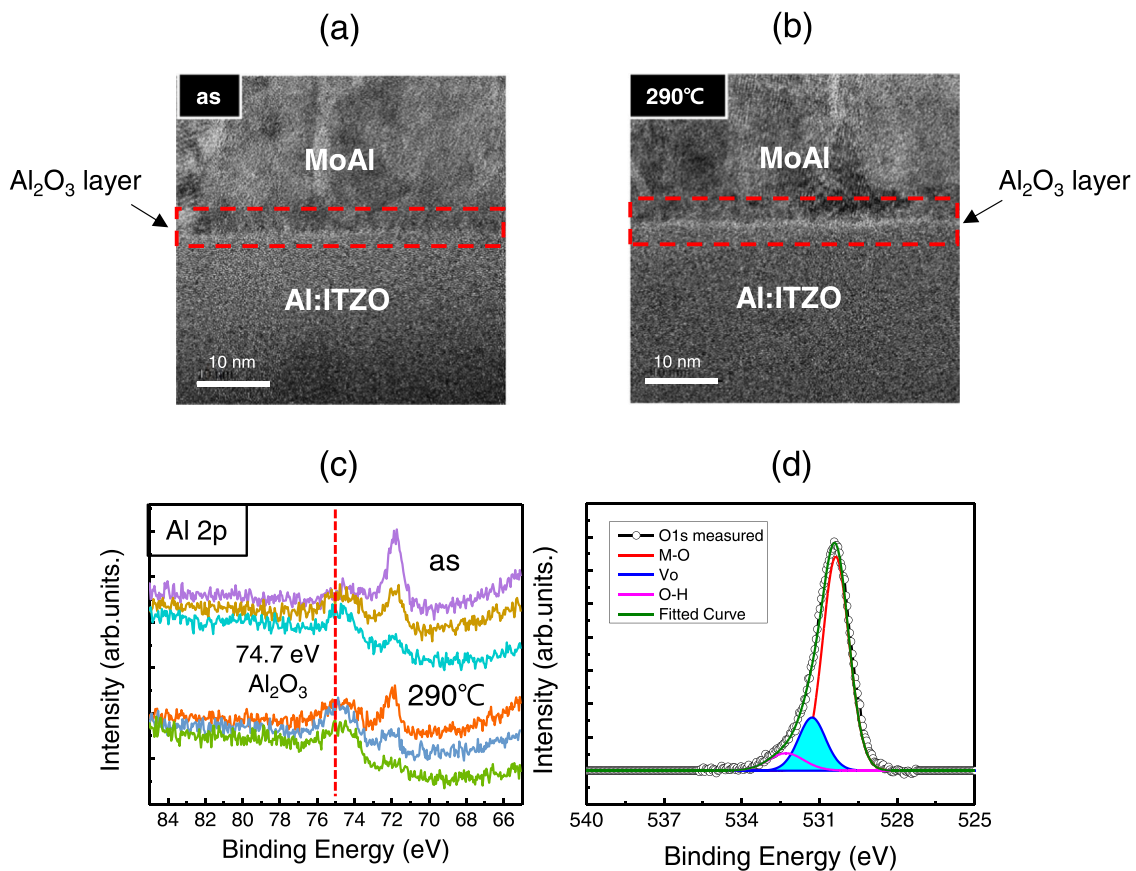


Fig. 8. Cross-sectional TEM images of the (a) as-deposited Mo–Al/Al:ITZO interfaces and (b) Mo–Al/Al:ITZO interfaces annealed at 290 °C. (c) Al 2p and (d) O1s level spectra of the XPS depth profiles measured at Mo–Al/Al:ITZO interfaces for the as-deposited and annealed at 290 °C.

suppresses the hydrogen diffusion into the Al:ITZO active layer from the S/D region. To investigate the oxygen vacancy (V_o) generated during the formation of Al_2O_3 interfacial layer, XPS depth spectra for O1s were measured at Mo–Al/Al:ITZO interface annealed at 250 °C. The Mo–Al/Al:ITZO sample showed the area ratio related to the oxygen-deficient (V_o) region of 21.03%, which was a slightly higher value compared to that of Mo/Al:ITZO sample (19.67%), and lower than that of Mo–Ti/Al:ITZO sample (22.02%). The measured area related to the oxygen-deficient region (V_o) showed little difference regardless of the Cu barrier electrodes (Mo, Mo–Ti, and Mo–Al), while the ΔV_{on} and ΔL differences were too large. Therefore, oxygen vacancies formed at the interfaces between the Cu barrier electrodes (Mo, Mo–Ti, and Mo–Al) and the Al:ITZO layer did not act as the major source of different carrier concentration.

To investigate the effect of Al_2O_3 layer formed at the Mo–Al/Al:ITZO interface on the electrical contact property, we measured the output characteristics at small V_D ($V_D = -1\text{ V} \sim 1\text{ V}$). Since Al_2O_3 layer is denser and thicker at the annealing temperature of 290 °C, output curve was observed in the device annealed at 290 °C. As shown in Fig. 9a, it shows typical behavior of output curve with no current crowding. In addition, we extracted the contact resistance (R_c) in detail using the “paired V_G ” method at each $V_G - V_{ON}$ [52]. Using the intersection of V_G and $V_G + \Delta V_G$ lines, the contact resistance (R_c) at each $V_G - V_{ON}$ was measured for the device C (Mo–Al) and device A, B (Mo, Mo–Ti) annealed at 290 °C, as shown in Fig. 9b. All devices show similar results and the contact resistance decrease with increasing $V_G - V_{ON}$. Therefore, it confirmed that contact issue was not investigated, which originate from the tunneling mechanism that electron can pass through the ultra-thin Al_2O_3 (~1 nm) layer. The contact resistance with various channel lengths depending on Cu diffusion barriers are obtained from the each point in TLM

results. The total contact resistance of device A, B, and C are similar, thus, we confirmed that Cu diffusion barrier materials do not affect the resistance of the Al:ITZO TFT.

To observe the H and OH diffusion from the Mo–Al (Cu diffusion barrier) to the Al:ITZO layer, SIMS measurements were performed and compared with the results of Mo and Mo–Ti (Fig. 9c, d, and e). From the SIMS depth profile results, the Al:ITZO layer with a Mo–Al (Cu diffusion barrier) contained a minimum amount of –OH as compared to those of other samples with Mo and Mo–Ti. In addition, the –OH peak intensity hardly changed with the increasing annealing temperature. The results suggested that applying Mo–Al alloy as a Cu diffusion barrier can suppress the diffusion of hydrogen from S/D to the active layer, thereby achieving excellent properties for the channel-shortening effect.

The transfer curve under positive-bias temperature stress (PBTS) and negative-bias stress (NBS) conditions were measured over 10,000 s, as shown in Fig. 10. During the PBTS conditions, the applied gate bias and temperature were 10 V (1 MV/cm) and 60 °C, respectively. Device C (Mo–Al) shows excellent stability and V_{on} shifting by only 0.28 V. In addition, under the NBS (–1 MV/cm, 10,000 s), it also exhibited stable performance, showing a V_{on} shift value of –0.25 V. PBTS stability is generally affected by electrons trapped at the interface between the gate insulator (GI) and active layer, and environmental influence. Oxygen absorption induces electron depletion from the channel layer, degrading the device electrical stability. In addition, the meta-stable gap state induced by water (H_2O) molecules could affect the negative bias stress (NBS) stability [53–55]. However, device C (Mo–Al) was not affected by the environmental influences because the top-gate coplanar self-aligned structure TFT was adopted in this experiment. Especially, pre-annealing process performed at 330 °C during the device fabrication

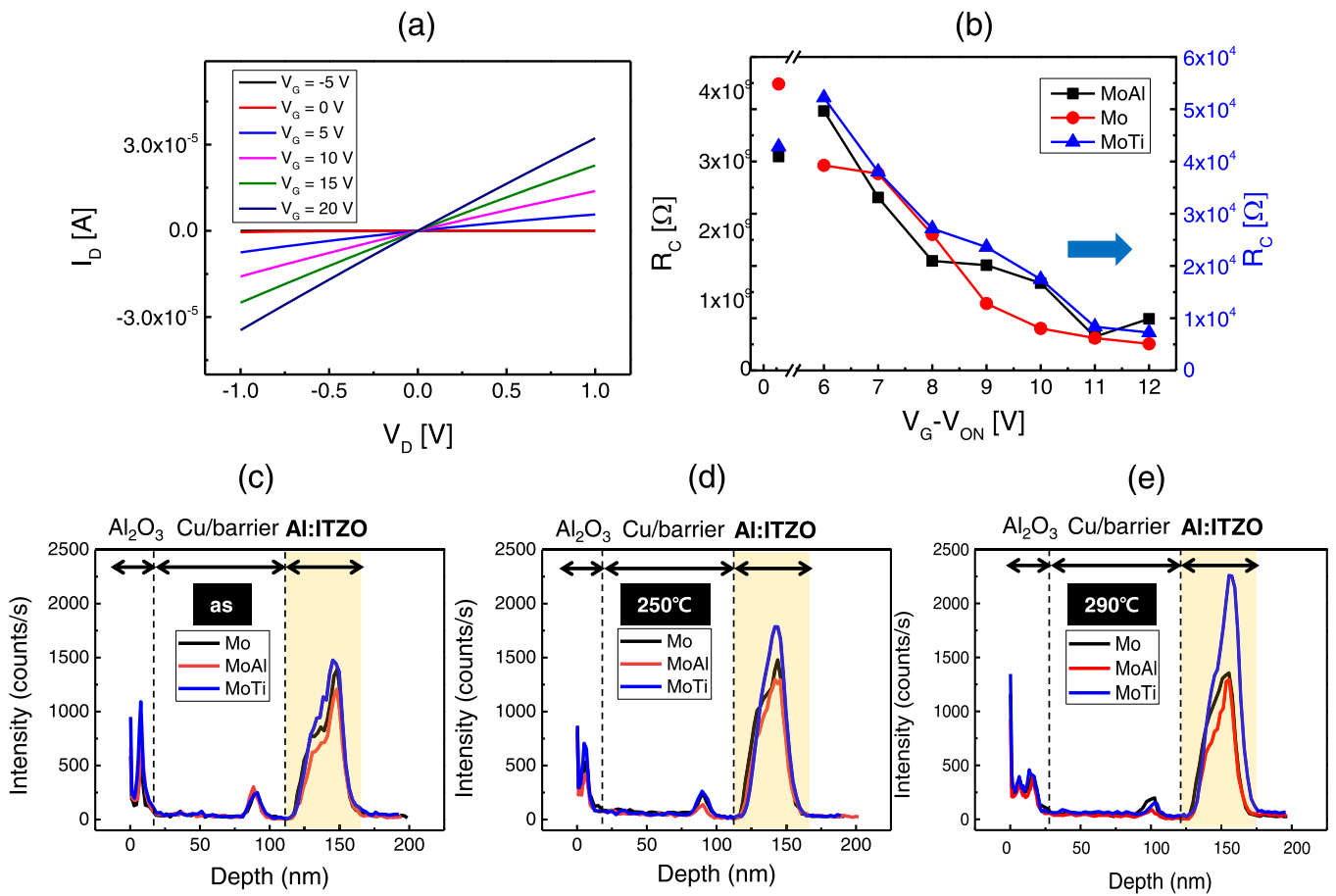


Fig. 9. (a) Output characteristics of device C (Mo-Al) annealed at 290 °C and (b) contact resistance of device A (Mo), B (Mo-Ti), and C (Mo-Al) annealed at 290 °C. Depth profile of -OH element in (c) as-deposited stacked film and after thermal annealing process at a temperature of (d) 250 °C and (e) 290 °C.

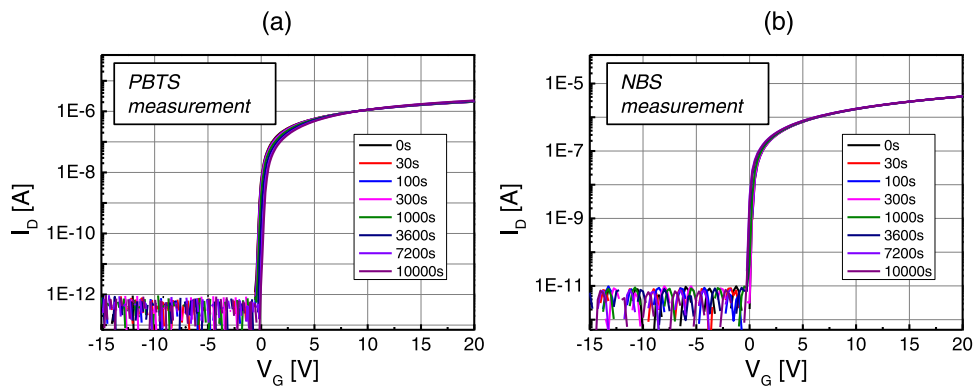


Fig. 10. Transfer curve during (a) PBTS and (b) NBS measurement of TFT with Mo-Al electrode.

allows the passivation of interface traps by the hydrogen, diffused from the GI layer. This enabled the device to exhibit excellent stability. Therefore, TFTs with Cu/Mo-Al source/drain electrodes can be potential candidates for the backplane devices of AMOLEDs with stable characteristics against channel-shortening effect as well as excellent stress stability.

4. Conclusion

In this paper, we introduced Mo-Al alloy as a Cu diffusion barrier in the S/D region of self-aligned Al:ITZO TFTs to minimize the channel-shortening effect. The effects of the Cu diffusion barrier on the channel-

shortening length was investigated using molybdenum and molybdenum alloys. From the experiments, we exploited the fact that hydrogen diffusion from the S/D region is the cause of the channel-shortening length (ΔL). Al_2O_3 passivation layer is the major source of hydrogen in the case of TFTs with Mo (Cu diffusion barrier). Furthermore, with the Mo-Ti (Cu diffusion barrier), both, the Al_2O_3 layer and Mo-Ti alloy became the source of hydrogen. This is due to the high solubility of hydrogen in the Mo-Ti alloy, which induces the hydrogen diffusion into the Al:ITZO active layer. Therefore, TFT with a Mo-Al (Cu diffusion barrier) exhibits improved characteristics to the channel-shortening effect by forming an ultra-thin Al_2O_3 layer at the Al:ITZO interface, preventing the hydrogen diffusion into the Al:ITZO active layer.

Furthermore, ΔV_{on} and ΔL with annealing temperatures were derived from the transfer characteristics and TLM method, respectively, showing the smallest value. This study demonstrated that the channel-shortening length can be modulated by changing the Cu diffusion barriers, thus realizing TFTs that works stably at short channel lengths.

CRediT authorship contribution statement

Wooseok Jeong: Conceptualization, Methodology, Investigation, Formal analysis, Investigation, Visualization, Writing - original draft, Writing - review & editing. **Jörg Winkler:** Methodology, Investigation, Resources, Validation. **Hennrik Schmid:** Methodology, Resources, Investigation. **Kwang heum Lee:** Methodology, Resources, Investigation. **Sang-Hee Ko Park:** Supervision, Resources, Project administration, Funding acquisition, Writing - review & editing.

Declaration of competing interest

The authors declare that they have no known competing financial interests or personal relationships that could have appeared to influence the work reported in this paper.

Acknowledgements

This work was supported by the National Research Foundation of Korea (NRF) grant funded by the Korea government (MSIT) (2018R1A2A3075518).

Appendix A. Supporting information

Supplementary data associated with this article can be found in the online version at [doi:10.1016/j.jallcom.2020.158227](https://doi.org/10.1016/j.jallcom.2020.158227).

References

- [1] K. Nomura, H. Ohta, A. Takagi, T. Kamiya, M. Hirano, H. Hosono, Room-temperature fabrication of transparent flexible thin-film transistors using amorphous oxide semiconductors, *Nature* 432 (2004) 488–492, <https://doi.org/10.1038/nature03090>
- [2] K. Nomura, A. Takagi, T. Kamiya, H. Ohta, M. Hirano, H. Hosono, Amorphous oxide semiconductors for high-performance flexible thin-film transistors, *Jpn. J. Appl. Phys.* 1 (45) (2006) 4303–4308, <https://doi.org/10.1143/JJAP.45.4303>
- [3] Y.L. Wang, F. Ren, W. Lim, D.P. Norton, S.J. Pearton, I.I. Kravchenko, J.M. Zavada, Room temperature deposited indium zinc oxide thin film transistors, *Appl. Phys. Lett.* 90 (2007) 232103, <https://doi.org/10.1063/1.2746084>
- [4] G. He, J.W. Liu, H.S. Chen, Y.M. Liu, Z.Q. Sun, X.S. Chen, M. Liu, L.D. Zhang, Interface control and modification of band alignment and electrical properties of HfTiO/GaAs gate stacks by nitrogen incorporation, *J. Mater. Chem. C* 2 (2014) 5299–5308, <https://doi.org/10.1039/C4TC00572D>
- [5] G. He, J. Gao, H.S. Chen, J.B. Cui, Z.Q. Sun, X.S. Chen, Modulating the interface quality and electrical properties of HfTiO/InGaAs Gate stack by atomic-layer-deposition-derived Al₂O₃ passivation layer, *ACS Appl. Mater. Interfaces* 6 (2014) 22013–22025, <https://doi.org/10.1021/am506351u>
- [6] J.W. Zhang, G. He, L. Zhou, H.S. Chen, X.S. Chen, X.F. Chen, B. Deng, J.G. Lv, Z.Q. Sun, Microstructure optimization and optical and interfacial properties modulation of sputtering-derived HfO₂ thin films by TiO₂ incorporation, *J. Alloy. Compd.* 611 (2014) 253–259, <https://doi.org/10.1016/j.jallcom.2014.05.074>
- [7] G. He, X.S. Chen, Z.Q. Sun, Interface engineering and chemistry of Hf-based high-k dielectrics on III-V substrates, *Surf. Sci. Rep.* 68 (2013) 68–107, <https://doi.org/10.1016/j.surfrep.2013.01.002>
- [8] J.B. Ko, H.I. Yeom, S.H.K. Park, Plasma-enhanced atomic layer deposition processed SiO₂ gate insulating layer for high mobility top-gate structured oxide thin-film transistors, *IEEE Electron. Device Lett.* 37 (2016) 39–42, <https://doi.org/10.1109/LED.2015.2504931>
- [9] H.I. Yeom, J.B. Ko, G. Mun, S.H.K. Park, High mobility polycrystalline indium oxide thin-film transistors by means of plasma-enhanced atomic layer deposition, *J. Mater. Chem. C* 4 (2016) 6873–6880, <https://doi.org/10.1039/C6TC00580B>
- [10] C.Z. Mitsuru Nakata, Jerzy Kanicki, DC sputtered amorphous In-Sn-Zn-O thin-film transistors: electrical properties and stability, *Solid State Electron.* 110 (2016) 22–29, <https://doi.org/10.1016/j.sse.2015.11.025>
- [11] S.H. Cho, J.B. Ko, M.K. Ryu, J.H. Yang, H.I. Yeom, S.K. Lim, C.S. Hwang, S.H.K. Park, Highly stable, high mobility Al:SnZnInO back-channel etch thin-film transistor fabricated using PAN-based wet etchant for source and drain patterning, *IEEE Trans. Electron. Devices* 62 (2015) 3653–3657, <https://doi.org/10.1109/TED.2015.2479592>
- [12] S. Yang, D.H. Cho, M.K. Ryu, S.H.K. Park, C.S. Hwang, J. Jang, J.K. Jeong, Improvement in the photon-induced bias stability of Al-Sn-Zn-In-O thin film transistors by adopting AlO_x passivation layer, *Appl. Phys. Lett.* 96 (2010) 213511, <https://doi.org/10.1063/1.3432445>
- [13] J.B. Su, Y. Wang, Y.B. Ma, Q. Wang, L.J. Tian, S.Q. Dai, R. Li, X.Q. Zhang, Y.S. Wang, Preparation and electrical characteristics of N-doped In-Zn-Sn-O thin film transistors by radio frequency magnetron sputtering, *J. Alloy. Compd.* 750 (2018) 1003–1006, <https://doi.org/10.1016/j.jallcom.2018.04.058>
- [14] J.J. Jia, Y. Torigoshi, A. Suko, S. Nakamura, E. Kawashima, F. Utsuno, Y. Shigesato, Effect of nitrogen addition on the structural, electrical, and optical properties of In-Sn-Zn oxide thin films, *Appl. Surf. Sci.* 396 (2017) 897–901, <https://doi.org/10.1016/j.apsusc.2016.11.058>
- [15] D.H. Kang, I. Kang, S.H. Ryu, J. Jang, Self-aligned coplanar a-IGZO TFTs and application to high-speed circuits, *IEEE Electron. Device Lett.* 32 (2011) 1385–1387, <https://doi.org/10.1109/LED.2011.2161568>
- [16] D. Geng, D.H. Kang, M.J. Seok, M. Mativenga, J. Jang, High-speed and low-voltage-driven shift register with self-aligned coplanar a-IGZO TFTs, *IEEE Electron. Device Lett.* 33 (2012) 1012–1014, <https://doi.org/10.1109/LED.2012.2194133>
- [17] S.Y. Hong, H.J. Kim, D.H. Kim, H.Y. Jeong, S.H. Song, I.T. Cho, J. Noh, P.S. Yun, S.W. Lee, K.S. Park, S. Yoon, I.B. Kang, H.I. Kwon, Study on the lateral carrier diffusion and source-drain series resistance in self-aligned top-gate coplanar InGaZnO thin-film transistors, *Sci. Rep.* 9 (2019) 6588, <https://doi.org/10.1038/s41598-019-43186-7>
- [18] J.W. Lim, M. Isshiki, Electrical resistivity of Cu films deposited by ion beam deposition: effects of grain size, impurities, and morphological defect, *J. Appl. Phys.* 99 (2006) 094909, <https://doi.org/10.1063/1.2194247>
- [19] C.C. Yang, T. Spooner, P. McLaughlin, R. Quon, T. Standaert, D. Edelstein, Via resistance reduction in advanced copper interconnects, *IEEE Electron. Device Lett.* 38 (2017) 115–118, <https://doi.org/10.1109/LED.2016.2628813>
- [20] F. Thiery, Y. Pauleau, L. Ortega, Effect of the substrate bias voltage on the physical characteristics of copper films deposited by microwave plasma-assisted sputtering technique, *J. Vac. Sci. Technol. A* 22 (2004) 30–35, <https://doi.org/10.1116/1.1626643>
- [21] P.C. Andriacos, Copper On-Chip, Interconnections, *Electrochem. Soc. Interfaces* 8 (1999) 32 (<https://www.electrochem.org/dl/interface/spr/spr99/IF3-99-Pages32-37.pdf>).
- [22] W.S. Kim, Y.K. Moon, K.T. Kim, J.H. Lee, B.D. Ahn, J.W. Park, An investigation of contact resistance between metal electrodes and amorphous gallium-indium-zinc oxide (a-GIZO) thin-film transistors, *Thin Solid Films* 518 (2010) 6357–6360, <https://doi.org/10.1016/j.tsf.2010.02.044>
- [23] W.S. Kim, Y.K. Moon, S. Lee, B.W. Kang, T.S. Kwon, K.T. Kim, J.W. Park, Copper source/drain electrode contact resistance effects in amorphous indium-gallium-zinc-oxide thin film transistors, *Phys. Status Solidi RRL* 3 (2009) 239–241, <https://doi.org/10.1002/pssr.200903225>
- [24] J.R. Yim, S.Y. Jung, H.W. Yeon, J.Y. Kwon, Y.J. Lee, J.H. Lee, Y.C. Joo, Effects of metal electrode on the electrical performance of amorphous In-Ga-Zn-O thin film transistor, *Jpn. J. Appl. Phys.* 51 (2012) 011401, <https://doi.org/10.1143/JJAP.51.011401>
- [25] Y.H. Tai, H.L. Chiu, L.S. Chou, The deterioration of a-IGZO TFTs owing to the copper diffusion after the process of the source/drain metal formation, *J. Electrochem. Soc.* 159 (2012) J200–J203, <https://doi.org/10.1149/2.025206jes>
- [26] B.O. Kim, J.H. Kim, H. Choe, J.H. Jeon, J.H. Seo, Characteristic of BCE Type IGZO thin film transistor device with various source/drain metals, *J. Nanosci. Nanotechnol.* 17 (2017) 8582–8586, <https://doi.org/10.1166/jnn.2017.15162>
- [27] L.Y. Kim, O.K. Kwon, Effects of stacked Mo-Ti/Cu source and drain electrodes on the performance of amorphous In-Ga-Zn-O thin-film transistors, *IEEE Electron. Device Lett.* 39 (2018) 43–46, <https://doi.org/10.1109/LED.2017.2769669>
- [28] K.H. Choi, H.K. Kim, Correlation between Ti source/drain contact and performance of InGaZnO-based thin film transistors, *Appl. Phys. Lett.* 102 (2013) 052103, <https://doi.org/10.1063/1.4790357>
- [29] H.W. Kim, E.S. Kim, J.S. Park, J.H. Lim, B.S. Kim, Influence of effective channel length in self-aligned coplanar amorphous-indium-gallium-zinc-oxide thin-film transistors with different annealing temperatures, *Appl. Phys. Lett.* 113 (2018) 022104, <https://doi.org/10.1063/1.5027373>
- [30] M. Nakata, M. Ochi, H. Tsuji, T. Takei, M. Miyakawa, T. Yamamoto, H. Goto, T. Kugimiya, Y. Fujisaki, A method for shortening effective channel length in oxide TFT by partial formation of conductive region, *Jpn. J. Appl. Phys.* 58 (2019) 090602, <https://doi.org/10.7567/1347-4065/ab12f1>
- [31] M.K. Song, S.H. Kuk, Y.W. Lee, M.K. Han, Oxygen Vacancy Diffusion in amorphous In-Ga-Zn-Oxide Thin-film-Transistors with Ti/Cu Source/Drain, 2012 19th International Workshop on Active-Matrix Flatpanel Displays and Devices (AMFPD): TFT Technologies and FPD Materials, (2012) 17–20. (<https://ieeexplore.ieee.org/stamp/stamp.jsp?tp=&arnumber=6294888>).
- [32] J.S. Park, T.S. Kim, K.S. Son, E. Lee, J.S. Jung, K.H. Lee, W.J. Maeng, H.S. Kim, E.S. Kim, K.B. Park, J.Y. Kwon, M.K. Ryu, S.Y. Lee, Ti/Cu bilayer electrodes for SiNx-passivated Hf-In-Zn-O thin film transistors: device performance and contact resistance, *Appl. Phys. Lett.* 97 (2010) 162105, <https://doi.org/10.1063/1.3505151>
- [33] T. Arai, N. Morosawa, K. Tokunaga, Y. Terai, E. Fukumoto, T. Fujimori, T. Sasaoka, Highly reliable oxide-semiconductor TFT for AMOLED displays, *J. Soc. Inf. Disp.* 19 (2011) 205–211, <https://doi.org/10.1889/JSID19.2.205>
- [34] H. Kitakado, S. Katoh, Channel shortening phenomenon due to redox reaction in a lateral direction on In-Ga-Zn-O thin film transistors, *Jpn. J. Appl. Phys.* 51 (2012) 03CB02, <https://doi.org/10.1143/JJAP.51.03CB02>
- [35] J. Kataoka, N. Saito, T. Ueda, T. Tezuka, T. Sawabe, K. Ikeda, Tungsten/In-Sn-O stacked source/drain electrode structure of In-Ga-Zn-O thin-film transistor for low-contact resistance and suppressing channel shortening effect, *Jpn. J. Appl. Phys.* 58 (2019) SBBJ03, <https://doi.org/10.7567/1347-4065/aaf97>

- [36] X.D. Huang, J.Q. Song, P.T. Lai, Improved performance of scaled-down alpha-InGaZnO thin-film transistor by Ar plasma treatment, *IEEE Electron. Device Lett.* 37 (2016) 1574–1577, <https://doi.org/10.1109/LED.2016.2615879>
- [37] H.H. Berger, Models for contacts to planar devices, *Solid State Electron.* 15 (1972) 145–158, [https://doi.org/10.1016/0038-1101\(72\)90048-2](https://doi.org/10.1016/0038-1101(72)90048-2)
- [38] E.N. Cho, J.H. Kang, I. Yun, Contact resistance dependent scaling-down behavior of amorphous InGaZnO thin-film transistors, *Curr. Appl. Phys.* 11 (2011) 1015–1019, <https://doi.org/10.1016/j.cap.2011.01.017>
- [39] S. Iwamatsu, K. Takechi, T. Yahagi, Y. Watanabe, H. Tanabe, S. Kobayashi, Depth-profiling study on amorphous indium-gallium-zinc oxide thin-film transistors by X-ray photoelectron spectroscopy, *Jpn. J. Appl. Phys.* 52 (2013) 03BB03, <https://doi.org/10.7567/JJAP.52.03BB03>
- [40] N.H. Nickel, Hydrogen transport properties in zinc oxide, *Superlattices Microstruct.* 42 (2007) 3–7, <https://doi.org/10.1016/j.spmi.2007.04.044>
- [41] H.K. Noh, J.S. Park, K.J. Chang, Effect of hydrogen incorporation on the negative bias illumination stress instability in amorphous In-Ga-Zn-O thin-film transistors, *J. Appl. Phys.* 113 (2013) 063712, <https://doi.org/10.1063/1.4792229>
- [42] X.C. Li, Li, Liang Wang, Changyuan Tao, Xiaoping Wu, Jun Du, Zuohua Liu, Synthesis of Ti^{3+} self-doped mesoporous TiO_2 cube with enhanced visible-light photoactivity by a simple reduction method, *J. Alloys Compd.* 845 (2020) 156138, <https://doi.org/10.1016/j.jallcom.2020.156138>
- [43] Y.W. Lee, S.J. Kim, S.Y. Lee, W.G. Lee, K.S. Yoon, J.W. Park, J.Y. Kwon, M.K. Han, Effect of Ti/Cu source/drain on an amorphous IGZO TFT employing SiN_x passivation for low data-line resistance, *Electrochem. Solid State Lett.* 15 (2012) H126–H129, <https://doi.org/10.1149/2.003205esl>
- [44] C. Oh, H. Jang, H.W. Kim, H. Jung, H. Park, J. Cho, B.S. Kim, Influence of oxygen partial pressure in In-Sn-Ga-O thin-film transistors at a low temperature, *J. Alloy. Compd.* 805 (2019) 211–217, <https://doi.org/10.1016/j.jallcom.2019.07.091>
- [45] A. Abliz, Effects of hydrogen plasma treatment on the electrical performances and reliability of InGaZnO thin-film transistors, *J. Alloy. Compd.* 831 (2020) 154694, <https://doi.org/10.1016/j.jallcom.2020.154694>
- [46] T. Kamiya, K. Nomura, H. Hosono, Origins of high mobility and low operation voltage of amorphous oxide TFTs: electronic structure, electron transport, defects and doping, *J. Disp. Technol.* 5 (2009) 273–288, <https://doi.org/10.1109/JDT.2009.20345>
- [47] C.G. Van de Walle, Hydrogen as a cause of doping in zinc oxide, *Phys. Rev. Lett.* 85 (2000) 1012–1015, <https://doi.org/10.1103/PhysRevLett.85.1012>
- [48] L. Sun, W. Xiao, S.H. Huang, J.W. Wang, L.G. Wang, Improving the mechanical processing of titanium by hydrogen doping: a first-principles study, *Int. J. Hydrog. Energy* 43 (2018) 6756–6764, <https://doi.org/10.1016/j.ijhydene.2018.02.066>
- [49] J.B. Ko, S.H. Lee, K.W. Park, S.H.K. Park, Interface tailoring through the supply of optimized oxygen and hydrogen to semiconductors for highly stable top-gate-structured high-mobility oxide thin-film transistors, *RSC Adv.* 9 (2019) 36293–36300, <https://doi.org/10.1039/C9RA06960G>
- [50] E. Langereis, M. Creatore, S.B.S. Heil, M.C.M. Van de Sanden, W.M.M. Kessels, Plasma-assisted atomic layer deposition of Al_2O_3 moisture permeation barriers on polymers, *Appl. Phys. Lett.* 89 (2006) 081915, <https://doi.org/10.1063/1.2338776>
- [51] S.Y. Huang, T.C. Chang, M.C. Chen, S.C. Chen, C.T. Tsai, M.C. Hung, C.H. Tu, C.H. Chen, J.J. Chang, W.L. Liao, Effects of Ambient atmosphere on electrical characteristics of Al_2O_3 passivated InGaZnO thin film transistors during positive-bias-temperature-stress operation, *Electrochem. Solid State Lett.* 14 (2011) H177–H179, <https://doi.org/10.1149/1.3534828>
- [52] G.J. Hu, C. Chang, Y.T. Chia, Gate-voltage-dependent effective channel length and series resistance of Ldd mosfets, *IEEE Trans. Electron. Devices* 34 (1987) 2469–2475, <https://doi.org/10.1063/1.3521310>
- [53] A. Abliz, J.L. Wang, L. Xu, D. Wan, L. Liao, C. Ye, C.S. Liu, C.Z. Jiang, H.P. Chen, T.L. Guo, Boost up the electrical performance of InGaZnO thin film transistors by inserting an ultrathin InGaZnO:H layer, *Appl. Phys. Lett.* 108 (2016) 213501, <https://doi.org/10.1063/1.4952445>
- [54] A. Abliz, L. Xu, D. Wan, H.M. Duan, J.L. Wang, C.L. Wang, S.J. Luo, C.S. Liu, Effects of yttrium doping on the electrical performances and stability of ZnO thin-film transistors, *Appl. Surf. Sci.* 475 (2019) 565–570, <https://doi.org/10.1016/j.apsusc.2018.12.236>
- [55] A. Abliz, D. Wan, J.Y. Chen, L. Xu, J.W. He, Y.B. Yang, H.M. Duan, C.S. Liu, C.Z. Jiang, H.P. Chen, T.L. Guo, L. Liao, Enhanced reliability of In-Ga-ZnO thin-film transistors through design of dual passivation layers, *IEEE Trans. Electron. Devices* 65 (2018) 2844–2849, <https://doi.org/10.1109/JED.2018.2836146>